creative commons
COMMONS DEED

저작자표시-비영리-변경금지 2.0 대한민국

이용자는 아래의 조건을 따르는 경우에 한하여 자유롭게

- 이 저작물을 복제, 배포, 전송, 전시, 공연 및 방송할 수 있습니다.

다음과 같은 조건을 따라야 합니다:

저작자표시. 귀하는 원저작자를 표시하여야 합니다.

비영리. 귀하는 이 저작물을 영리 목적으로 이용할 수 없습니다.

변경금지. 귀하는 이 저작물을 개작, 변형 또는 가공할 수 없습니다.

- 귀하는, 이 저작물의 재이용이나 배포의 경우, 이 저작물에 적용된 이용허락조건을 명확하게 나타내어야 합니다.
- 저작권자로부터 별도의 허가를 받으면 이러한 조건들은 적용되지 않습니다.

저작권법에 따른 이용자의 권리는 위의 내용에 의하여 영향을 받지 않습니다.

이것은 이용허락규약(Legal Code)을 이해하기 쉽게 요약한 것입니다.

Disclaimer

dCollection

공학석사 학위논문

Layer-by-layer Cell Coating with Hydrogel Film for Cell Therapy

세포치료제를 위한 적층식 하이드로겔 필름 세포 코팅

2019 년 8 월

서울대학교 대학원
공과대학 화학생물공학부

김 민 지

ABSTRACT

Layer-by-layer Cell Coating with Hydrogel Film for Cell Therapy

Minji Kim
School of Chemical and Biological Engineering
The Graduate School of Engineering
Seoul National University

Cell therapy has been emerged as a promising approach for severe diseases. However, the efficacy of cell therapy is limited by low cell survival owing to external stress during and after transplantation. In this study, we constructed a layer-by-layer cell coating platform with hydrogel film that provides cells a cytoprotective barrier. The hydrogel film was stabilized by *Streptomyces avermitilis*-derived tyrosinase (SA-Ty) which mediate oxidative coupling reactions of mono-phenols. Hydrogel film-coated cells were characterized by measuring zeta potential, fluorescence intensity, and TEM imaging. The 6-layer stacked hydrogel film was as thick as 139.40 nm. Cell viability was not deteriorated by coating procedures. Furthermore, hydrogel film was fabricated on β-cell spheroids for the application in the field of islet transplantation. Confocal

image showed thin, uniform, and compact film layers on β-cell spheroids. In addition, hydrogel film-coated β-cell spheroids showed higher insulin secretion ability than the native β-cell spheroids. At last, the cytoprotective effects of the hydrogel film against physical and oxidative stress were evaluated *in vitro*. Overall, we expect our fast, facile, durable, and layer-controllable cell coating technique will offer a great potential for clinical applications in cell therapy.

Keyword: Cell therapy, Cell surface engineering, Islet encapsulation, Cytoprotection

Student Number: 2017-22285

Table of Contents

List of Figures and Table

Figures

Tables

Chapter 1. The Scientific Background and Research Progress

1.1 Cell Therapy

Cell therapy involves the transplantation of different types of cells, such as stem cells, T-cells, and pancreatic β-cells, into human body for the treatment of certain diseases or conditions [1, 2, 3]. For example, cardiac stem cells encapsulated in thermosensitive nanogel were transplanted to mouse and pig models of myocardial infarction (MI) [4]. Additionally, chimeric antigen receptor (CAR) T-cell therapy is currently implemented clinically in cancer immunotherapy which collect, genetically engineer, and infuse engineered autologous T-cells to the cancer patient in order to activate T-cell recognition of cancer cells. Furthermore, for the treatment of type 1 diabetes (T1D), allogeneic islet cells from brain-dead donor are encapsulated in alginate-based microbead and injected through portal vein [3]. In contrast to chemical drugs or biologics, delivering whole cell entities utilizes dynamic and environment-responsive cellular functions that is hard to be carried out with non-living materials. However, despite the exclusive advantages of the cell therapy, several challenges remain. Firstly, the survival rate of transplant cells is too low [5]. The cells encounter stress environments, such as high pressure due to direct injection, shear stress from blood circulation, and oxidative stress in inflammatory tissue. Secondly, the transplanted cells are hardly integrated into host tissue [6]. Lastly, allogeneic or xenogeneic cell transplantation triggers inflammatory host immune rejection [7, 8]. Therefore, cell protecting strategies which increase the efficacy of cell therapy are highly desired for the clinical application of cell therapy.

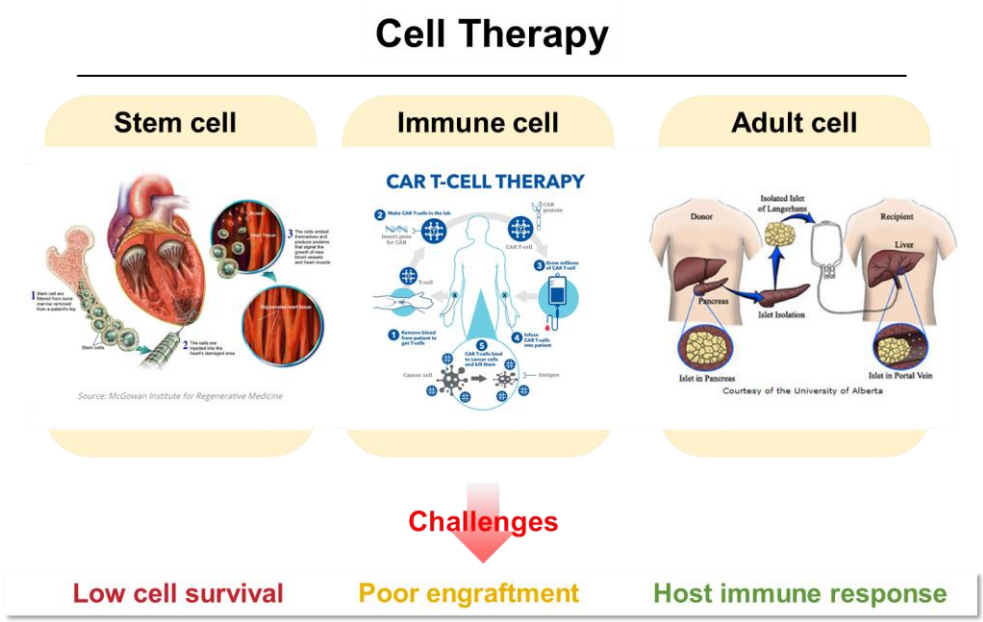

Figure 1.1 Overview of cell therapy classified by cell types and current clinical challenges.

1.2 Cell encapsulation for cell therapy

Cell encapsulation technologies has emerged as major solutions for above challenges [3, 9, 10]. Cells can be isolated from the environment via cell encapsulation with synthetic or natural materials, which protect cells and give extra functions to them [1]. Current cell encapsulation technologies include bulk hydrogel, microbead, hollow capsule, and cell surface engineering. Bulk hydrogel is usually constructed by *in-situ* gelation with injectable materials. After injection, the hydrogel forms its shape depending on the target site. This bulk hydrogel is usually used for topical delivery, for example, myocardial infarction, skin wound, or osteoarthritis. Cell microbead can be formed using microfluidics [11]. However, the limitation of bulk hydrogel and

microbead is the poor diffusion of oxygen and nutrients to the encapsulated cells due to the large volume of materials. Hollow capsule is developed for this reason. Microbeads (e.g. alginate beads) are coated with additional thin polymer shell followed by a treatment that selectively degrades inner hydrogel core (e.g. EDTA for alginate). Likewise, cell surface engineering, also known as cell coating or nanoencapsulation, is a nano-thin encapsulation strategy [3, 12]. This can be distinguished by a bottom-up approach. As the cell surface engineering exploits the properties of cell membrane, the methodology can be chemically, physically, and biologically developed.

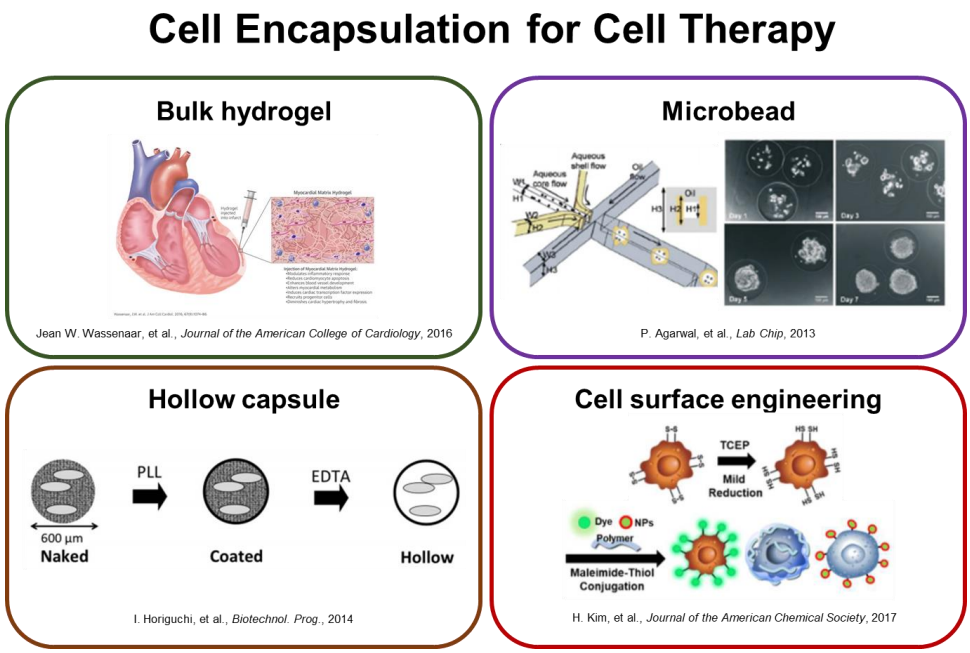

Figure 1.2 Overview of different types of cell encapsulation for cell therapy.

1.3 Strategies for cell surface engineering

The structure of cell membrane is highly complex and heterogeneous, displaying

diverse types of proteins, carbohydrates, and lipids. The strategies for cell surface engineering utilizes properties of these components. Electrostatic forces between the negatively charged cell membrane and positively charged polymer is one of the most researched method [13, 14]. Also, covalent bonds can be formed via click chemistry or maleimide-thiol chemistry, where the amine or thiol groups of the membrane proteins and carbohydrates are targeted [15]. Furthermore, functional groups can be introduced via membrane fusion with liposome owing to the characteristics of lipid bilayer [16]. Moreover, cell surface engineering has been achieved via various strategies, including nanoparticles, metabolic glycoengineering, and grafting-from polymerization [17, 18].

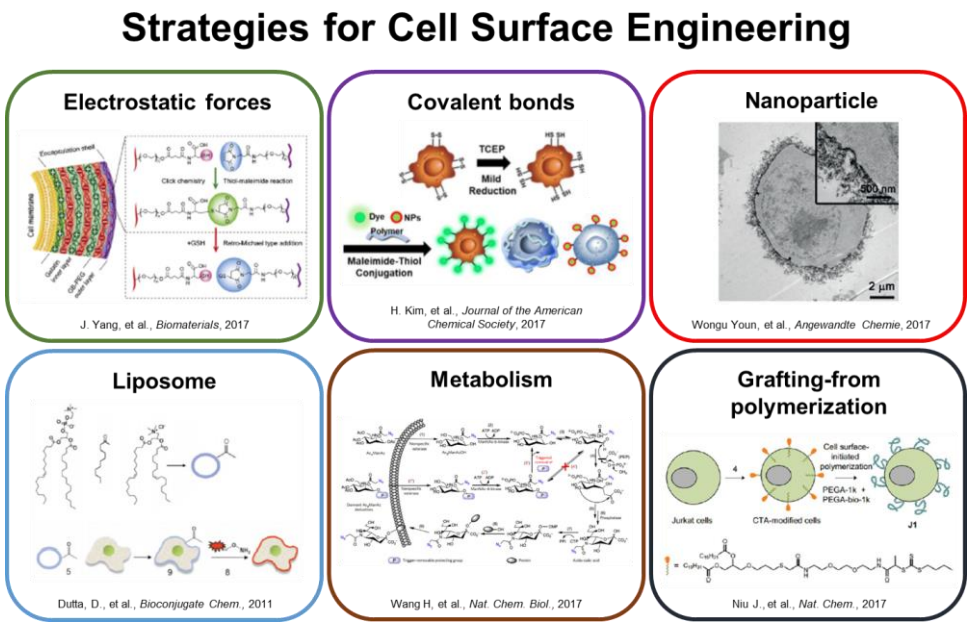

Figure 1.3 Overview of the strategies for cell surface engineering.

Chapter 2. Construction of Layer-by-layer (LbL) Cell Coating Platform

2.1 Introduction

Chitosan is a positively charged natural polysaccharide that is obtained by deacetylation of chitin from crustaceans. Hyaluronic acid is a negatively charged polysaccharide which is abundant in extracellular matrix (ECM) and has a high capacity of water absorption [19]. Tyrosinase is an enzyme that catalyzes a two-step oxidation of monophenols: *o*-hydroxylation of monophenols to *o*-diphenols and the subsequent oxidation to produce *o*-quinones [20]. A rapid forming hydrogel via tyrosinase crosslinking in physiological condition was reported in previous study [21, 22], where tyrosinase derived from *Streptomyces avermitilis* was used. Herein, we report a layer-by-layer cell coating platform that utilizes tyrosinase-mediated oxidative coupling reactions as well as electrostatic interactions between glycol chitosan and hyaluronic acid.

2.2 Materials and methods

2.2.1 Synthesis of GC-T, HA-T, GC-T-RITC, and HA-T-FA

4-Hydroxyphenylacetic acid (HPA) was conjugated to glycol chitosan (GC) via EDC/NHS coupling reaction as shown in Fig. 2.2. Firstly, 200 mg of GC were dissolved in 10 ml of 0.1M pH 4.7 MES buffer at 70 °C until fully dissolved. 160.82 mg of HPA were dissolved in 10 ml MES buffer, and 202.64 mg of EDC and 114.76 mg of NHS were added to the solution and stirred for 5 min. Then, two solutions were mixed and reacted overnight at RT. Next, the solution was dialyzed (SnakeSkin™ Dialysis Tubing, Mw cutoff 1 kDa, Thermo Fisher Scientific) against distilled water for 72 h and lyophilized for more than 72 h. In the same manner, HA-T was synthesized by conjugating tyramine hydrochloride to hyaluronic acid (HA). 200 mg of HA was dissolved in 20 ml of MES buffer, and 197.452 mg of EDC and 111.822 mg of NHS was added, stirred for 5 min. Then,178.85 mg of tyramine hydrochloride was added and reacted overnight at RT. Subsequently, the final solution was dialyzed and lyophilized. 1 ml of 10 mg/ml RITC and FA solution, dissolved in N,N-Dimethylformamide (DMF), was added to the reacting solution of GC-T and HA-T, respectively, to obtain GC-T-RITC and HA-T-FA.

2.2.2 Purification of recombinant tyrosinase from *Streptomyces avermitilis* (SA-Ty)

The recombinant plasmid for tyrosinase was constructed and provided by Professor

Byung-gee Kim (Seoul National University, Seoul, Korea). Briefly, the gene of tyrosinase (Ty) was extracted from Streptomyces avermitilis (SA) and His-tag was introduced at the C-terminal of Ty. For the protein expression and purification of SA-Ty, the plasmid was transformed into *E.coli* BL21 (DE3) by heat shock and selected on Luria-Bertani (LB) agar plate containing 100 μg/ml of ampicillin. A single colony was inoculated into 5 ml of LB broth with ampicillin and cultured overnight in a 37 ℃ shaking incubator at 200 rpm. Then, 2 ml of cell culture was transferred into a 1L flask with 200 ml of fresh LB containing 100 μg/ml of ampicillin. The cells were grown to an OD600 of 0.6 and protein expression induced by adding 0.2 mM IPTG and 1 mM $CuSO_4$. After 20 h at 18 ℃, cells were harvested by centrifugation at 4,000 rpm for 10 min at 4 ℃. Cell pellets were washed once and resuspended in 50 mM Tris-HCl buffer, pH 8.0, and disrupted by ultrasonication. Cell lysates were centrifuged at 15,000 rpm for 30 min at 4 ℃ to remove debris. The supernatant was collected and filtered through a sterilized 0.2 μm polyethersulfone membrane (Acrodisc® Syringe Filter with Supor® Membrane, Pall Life Sciences, USA). The enzyme was purified by the general His-tag purification using Ni-NTA agarose column (QIAGEN). The final enzyme solution was aliquoted and kept at -20 ℃ in pH 8.0 Tris-HCl buffer containing 25% glycerol. The concentration of purified SA-Ty was determined by Bradford assay.

2.2.3 Attenuated total reflection-fourier transform infrared spectrometer (ATR-FTIR)

0.1% GC-T and 0.1% HA-T solution was reacted with 0.05 U/ml SA-Ty for 30 min at RT. Then, reaction solution was frozen and lyophilized. The solid sample was directly

placed on the zinc selenide ATR crystal surface of ATR-FTIR (Spectrum 100 FT-IR Spectrometer, PerkinElmer, USA). The bare ATR crystal was used as a background. The FTIR spectra was obtained by scanning the transmittance at 700-4000 cm^{-1}.

2.2.4 Quartz crystal microbalance (QCM)

Cr/Au (Chromium/gold) crystal (5 MHz, 1 inch-diameter, AT-cut, plano-plano) was used to deposit GC-T/HA-T layers. Before the deposition, the crystal was treated with piranha solution (H2SO4:H2O2 = 3:1) for 5 min and oxygen plasma for 5 min to clean and set negative charge on the surface. Next, the crystal was soaked into the 0.1% GC-T solution with 0.05 U/ml SA-Ty. After 10 min, the electrode was rinsed twice with PBS for 1 min. To eliminate remaining PBS, the crystal was dried with air blower. LbL deposition was proceeded with 0.1% HA-T solution until total 5 bilayers were stacked. The hydrogel film deposited crystal was analyzed by QCM (QCM200, Stanford Research Systems, USA) for each layer.

2.2.5 Cell culture

Jurkat cells (Jurkat Clone E6-1, ATCC® TIB-152™) were cultured in 75 cm^2 tissue culture flasks with cell culture growth medium at 37 °C under humidified atmosphere containing 5% CO_2. The cell culture growth medium was RPMI 1640 containing 10% FBS and 1% PS. Cells were harvested by centrifugation at 1100 rpm for 5 min for subculture or experiments. Media was changed every 2 days. MIN6 β-cells were

cultured in high-glucose D-MEM containing 15% FBS, 1% PS, and 55 μM 2-ME and incubated in 5% CO2 at 37 °C. Media was changed every 2-3 days.

2.2.6 Hydrogel film coating on 2D cell surface

0.1% GC-T solution and 0.1% HA-T solution was prepared in PBS. MIN6 β-cells were seeded on 96-well tissue culture plate at a density of 2×10^4 cells. After 3 days, cells were washed twice with PBS for coating. Cells were incubated in GC-T or HA-T solution with SA-Ty for reaction time. Then, cells were washed twice with PBS to remove SA-Ty and medium components.

2.2.7 Layer-by-layer hydrogel film coating of single cells

Prior to encapsulation of cells, the activity of SA-Ty was measured. Lyophilized GC-T and HA-T was dissolved at 10 mg/ml in 0.1% acetic acid and PBS, respectively. After fully dissolved, the solutions were diluted 10 times with PBS, making final concentration of 1 mg/ml, and filtered through sterilized 0.2 μm membrane. Jurkat cells were collected, washed twice with PBS and prepared at the density of 1×10^7 cells per 1 ml of PBS. 100 μl of cell suspension were seeded into a 3.0 μm polycarbonate membrane (Transwell® 6.5 mm insert, 24-well plate, Corning®). After 600 μl of 1 mg/ml GC-T solution and 0.05 U/ml SA-Ty was added into a well of a 24-well plate, the cell seeded insert was dipped for 10 min at RT. During incubation, the plate was tapped every 2 min. After 10 min, the insert was transferred to a well with 500 ul of

media for 30 sec once and 500 ul of PBS for 1 min twice on a shaking incubator. Subsequently, HA-T and GC-T were applied alternatively in the same manner. When the last layer was finished, the cells were dispersed into cell culture medium.

2.2.8 Measurement of zeta potential

Cells were fixed with 4% paraformaldehyde (PFA) for 10 min and prepared at a density of 1×10^6 cells per 1 ml of PBS. The zeta potential of native or encapsulated cells were measured with Nano ZS (Malvern Instruments, Germany).

2.2.9 FACS analysis

Cells were encapsulated with GC-T-RITC and HA-T-FA instead of GC-T and HA-T. After fixing, cells were prepared at 1×10^6 cells per 500 μl of PBS. Fluorescence of RITC and FA was measured by a flow cytometry (FACS Aria II, BD Biosciences, USA) using lasers of wavelength of 488 nm and 633 nm. 1-layer encapsulated cells with GC-T-RITC and HA-T-FA were used as positive controls for gating.

2.2.10 Transmission electron microscopy (TEM)

To confirm the nanometer-thick hydrogel on the cell surface, TEM (Talos L120C, 120kV, FEI, Czech) image was analyzed. For the preparation of TEM sample, native

and encapsulated cells were fixed with Karnovsky's fixative. Cells were treated with 1% osmium tetroxide in cacodylate buffer for 1 h, 0.5% uranyl acetate overnight at 4 °C. After dehydrated in ethanol, the samples were embedded in Spurr's resin. The specimens were sectioned by using ultramicrotome (EM UC7, Leica, Germany).

2.2.11 Evaluation of cell viability and proliferation

Cell viability was measured by staining cells with Live/Dead® Viability/Cytotoxicity Kit that contains calcein-AM and ethidium homodimer-1 (EthD-1). After imaged with fluorescence microscope (EVOS® Cell Imaging Systems, Thermo Fisher Scientific), cells were counted in separate 4 fields to calculate the percentage of live cells. For proliferation, cell metabolism was measured for 3 or 4 days at 24 h-interval using alamarBlue® reagent. The measured fluorescence of the reagent was normalized to the value of the first day.

2.2.12 Statistical analysis

All data are expressed as mean ± standard deviation (SD). Statistical significance was determined by Student's t-test with * $p < 0.05$, ** $p < 0.01$, *** $p < 0.005$.

2.3 Results & Discussion

2.3.1 Synthesis and characterization of GC-T and HA-T

The EDC/NHS chemistry was used to introduce mono-phenolic groups into glycol chitosan (GC) and hyaluronic acid (HA) (Fig. 2.2). EDC/NHS chemistry is a coupling reaction of carboxylic acid group and amine group via activating carboxylic acid group with carbodiimide and amine-reactive sulfo-NHS ester. 4-Hydroxyphenylacetic acid (HPA), which is a monophenol with carboxylic group, and tyramine (Tyr), which is a monophenol with amine group, were used with GC and HA, respectively. The two mono-phenolic groups were referred to as 'T' in this study since tyramine conjugated HA was named HA-T in the previous study [20, 21]. GC, HPA, EDC and NHS were reacted with 2: 2: 2: 1 molar ratio, and HA, Tyr, EDC and NHS were reacted with 1: 2: 2: 1 molar ratio (Table 2.1) ^{1}H-NMR spectra of GC-T represented peaks at 6.791 and 7.100 ppm, while 6.847, 7.161, 7.272, 7.447 ppm on that of HA-T (Fig. 2.3). Degree of substitution (DS) was calculated as a function of the ratio of proton integration of T/GC or T/HA. DS of GC-T was 10.66%, and that of HA-T was 17.50% (Table 2.2). The zeta potential of 0.1% GC-T solution and 0.1% HA-T solution in PBS was 7.962 ± 1.457 mV and -17.392 ± 3.763 mV, respectively (Fig. 2.4).

2.3.2 Characterization of SA-Ty.

Cytotoxicity of SA-Ty was investigated for Jurkat cells (Fig. 2.5). SA-Ty was incubated at 0, 1.25, 2.5, and 5 μM for 10, 20, and 60 min on the media. After the wash, Live/Dead

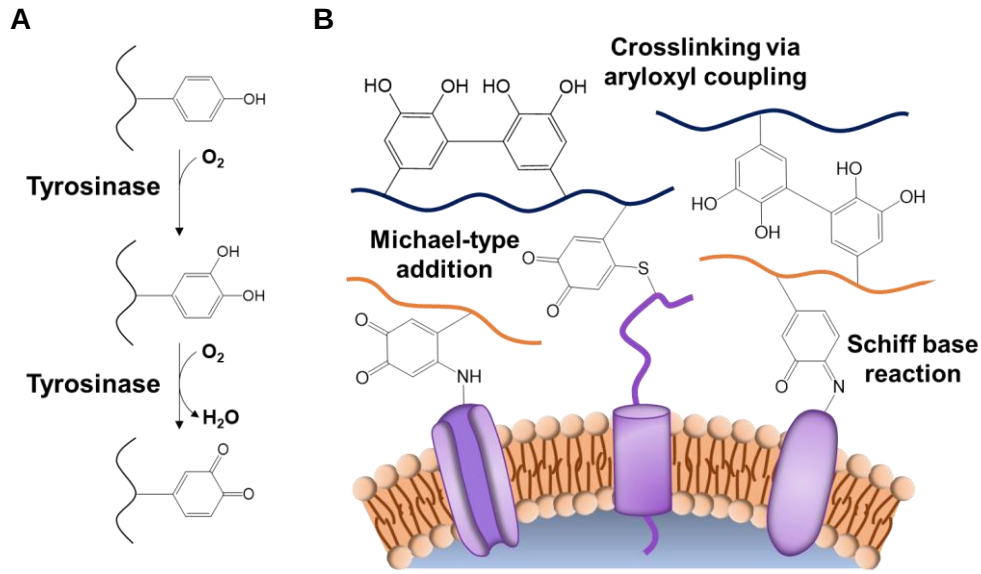

Figure 2.1 Schematic illustration of chemical reactions mediated by tyrosinase.

(A) Monophenol is subsequently oxidized to *o*-diphenol and *o*-quinone by tyrosinase with oxygen supply. (B) *O*-quinones form covalent bonds with amines and thiols on cell surface and crosslink via aryloxyl coupling.

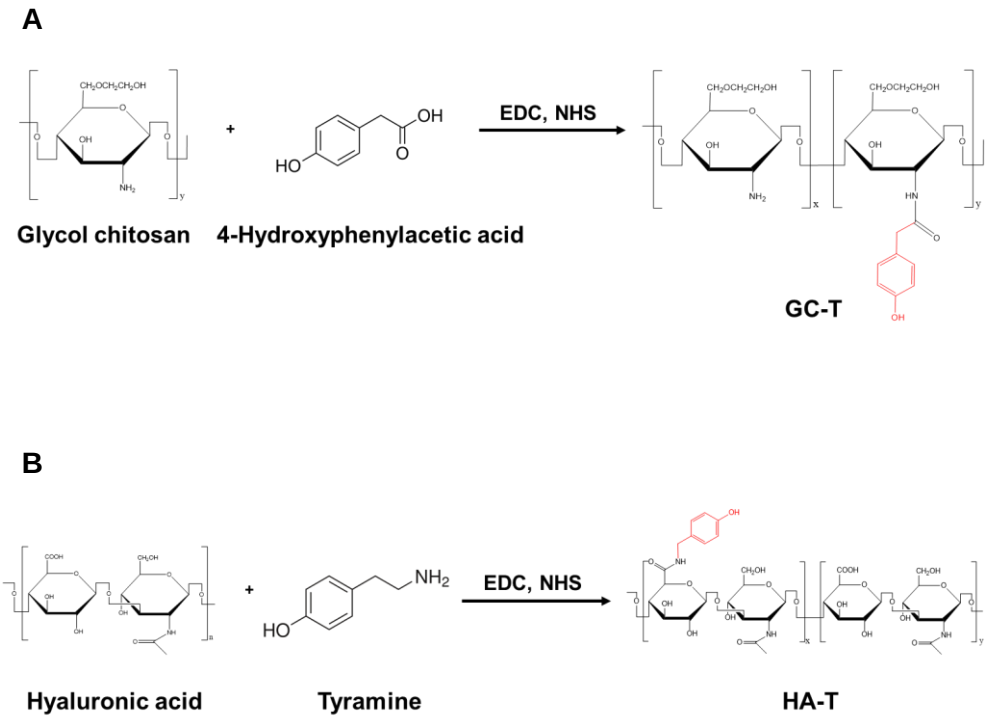

Figure 2.2 Schematic description of the chemical reactions of GC-T and HA-T.

(A) Glycol chitosan and 4-hydroxyphenylacetic acid were reacted to generate mono-phenolic groups on glycol chitosan (GC-T) via EDC/NHS chemistry. (B) Hyaluronic acid and tyramine were reacted to generate mono-phenolic group on hyaluronic acid (HA-T) in the same manner.

A

	GC	4-Hydroxyphenyl aceticacid	EDC	NHS
Functional Group	$[NH_2]$	[COOH]		
Molar ratio	2	2	2	1

B

	HA	Tyramine	EDC	NHS
Functional Group	[COOH]	$[NH_2]$		
Molar ratio	1	2	2	1

Table 2.1 Synthesis table of GC-T and HA-T via EDC/NHS chemistry used in this study.

Molar ratio of the reagents were considered for the synthesis of (A) GC-T and (B) HA-T.

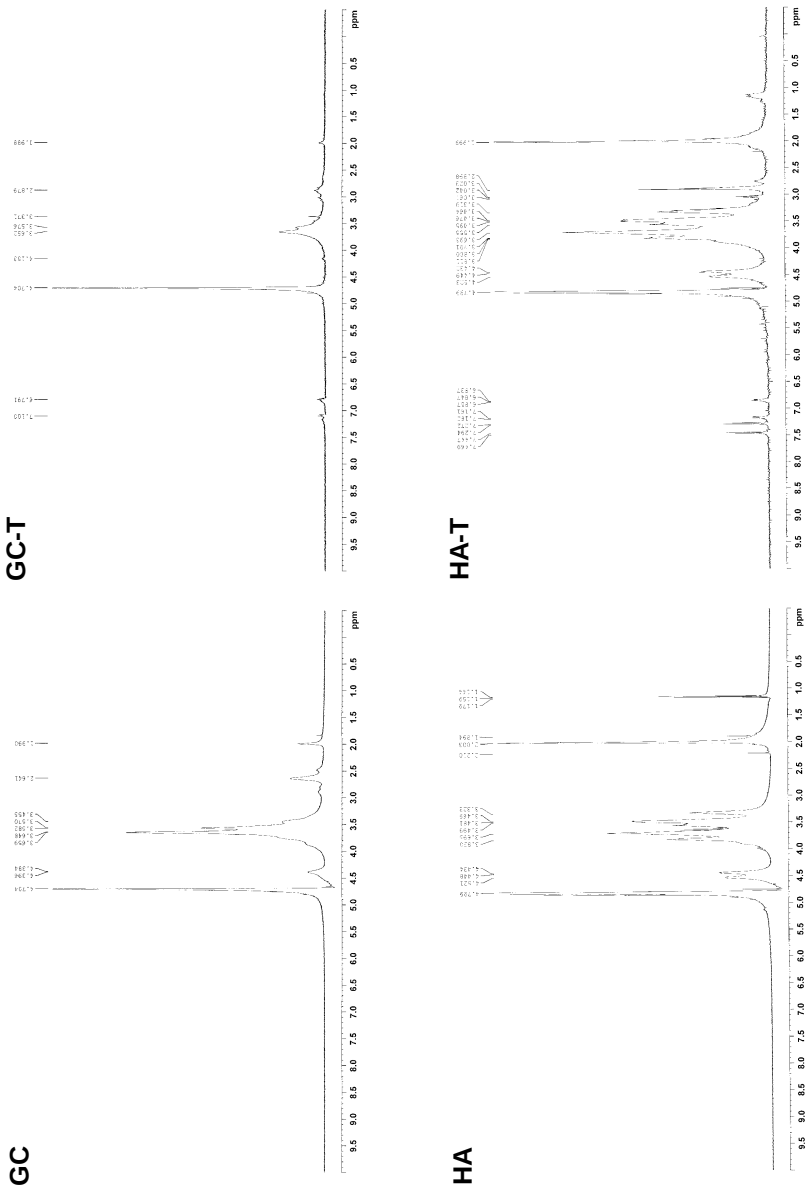

Figure 2.3 ^{1}H-NMR spectra.

Products from mono-phenolic group conjugation reaction showed peaks in 6.5-8.0 ppm.

A

GC-T

Chemical shift (in ppm)	integral	H (mol)	%
2.879	7.01	1	-
6.791	1.31	2	9.34
7.100	1.68	2	11.98
Degree of substitution			10.66

B

HA-T

Chemical shift (in ppm)	integral	H (mol)	%
1.999	3	3	-
6.847	0.17	1	17.00
7.161	0.16	1	16.00
7.272	0.18	1	18.00
7.447	0.19	1	19.00
Degree of substitution			17.50

Table 2.2 Degree of substitution (DS) as a function of the ratio of proton integration in T/GC or T/HA.

(A) DS of GC-T was calculated to 10.66%. (B) DS of HA-T was calculated to 17.50%.

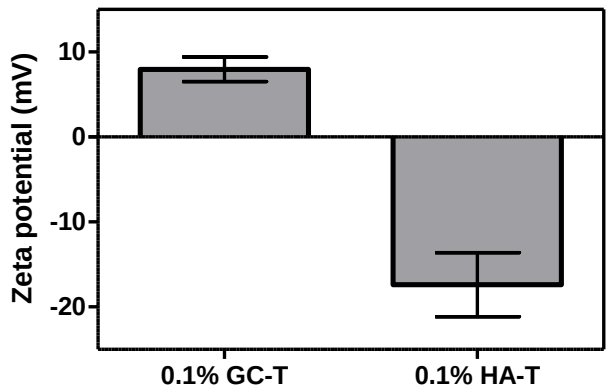

Figure 2.4 Zeta potential of 0.01% GC-T and 0.01% HA-T in PBS solution.

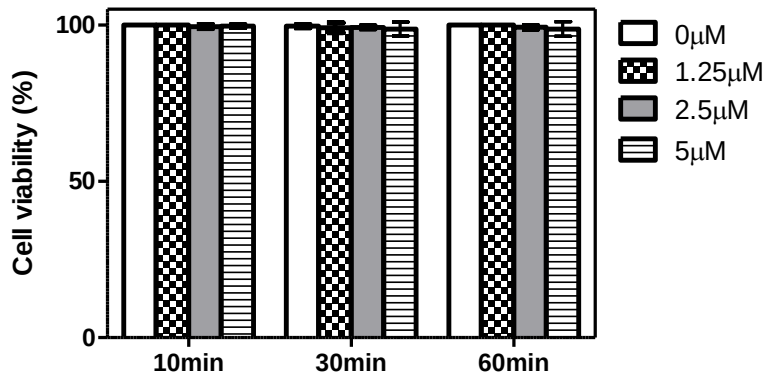

Figure 2.5 Cytotoxicity of SA-Ty on Jurkat cell calculated by Live/Dead assay (n=4).

assay was performed. The viability was calculated by dividing the live cell number by the total cell number. As a result, the viability of the whole group was over 98%. The catalytic activity of phenolic oxidation of SA-Ty was confirmed by UV-Vis spectrometer (Fig. 2.6). 1% GC-T and HA-T in PBS were used as substrates and $CuSO_4$ was added to measure the absorbance at 450 nm ($\varepsilon_{dopachrome}$ = 3600 $M^{-1}cm^{-1}$) with time. The concentration of dopachrome increased continuously over time, especially for HA-T, which showed a high velocity during the initial 3 min and then showed the same velocity as GC-T. The initial oxidation rate, V_0, of SA-Ty for 1% GC-T was 5.164 ± 1.598 μM/min, and V_0 for 1% HA-T was 24.576 ± 0.353 μM/min. After fully react substrates with SA-Ty by leaving at RT overnight, reacted solution was lyophilized, and then FT-IR spectra was obtained by ATR-FTIR (Fig 2.7). The broad peak of O-H bond at 3100-3500 cm^{-1} increased after phenolic oxidation, and the peak of aromatic C=C bond decreased at 1500-1800 cm^{-1}.

2.3.3 Optimization of hydrogel film coating conditions on 2D cell surface

Optimal hydrogel film coating conditions, including concentration of SA-Ty, reaction time, and concentration of polymers, were examined (Fig. 2.8). The degree of coating was confirmed by measuring fluorescence of GC-T-RITC and HA-T-FA. MIN6 β-cells seeded on 96-well tissue culture plate were incubated in 0.1% GC-T-RITC or HA-T-FA solution for 10 min with 0.05 U/ml SA-Ty. After washing with PBS, the intensity of fluorescence in two different regions was measured; one at λ_{ex} = 543 nm / λ_{em} = 580 nm (RITC) and the other at λ_{ex} = 495 nm / λ_{em} = 525 nm (FA). The concentration of SA-Ty showed the highest RITC intensity at 0.05 U/ml, where the reaction time was

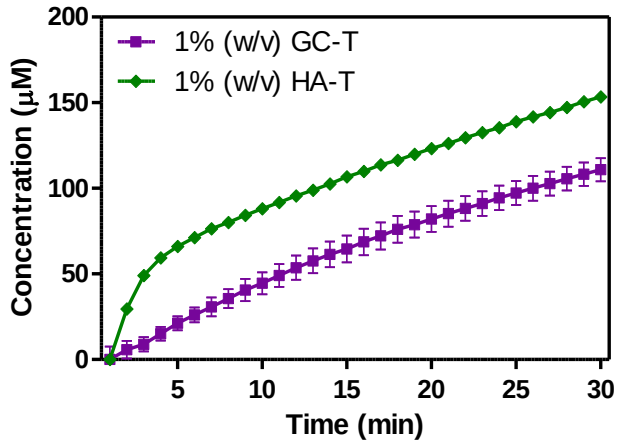

Figure 2.6 The catalytic enzyme activity test of phenolic oxidation of GC-T and HA-T mediated by SA-Ty (n=3).

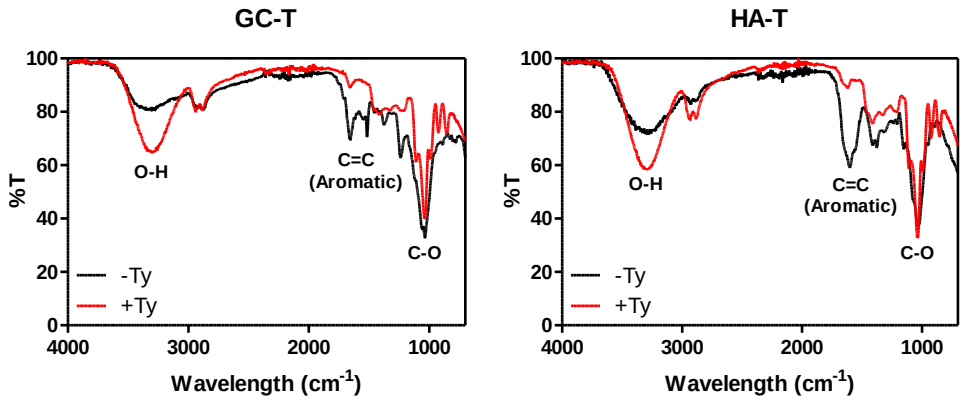

Figure 2.7 FT-IR spectra of (A) GC-T and (B) HA-T before and after SA-Ty reaction.

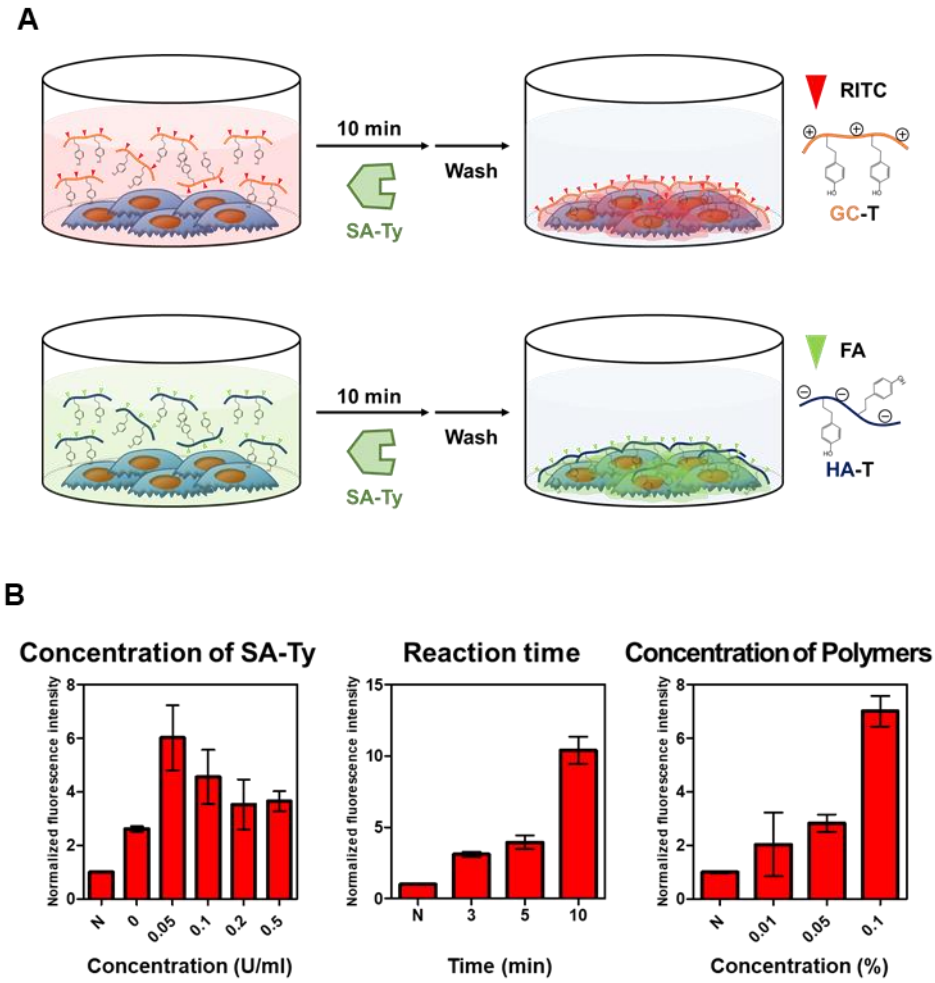

Figure 2.8 Optimization of hydrogel film coating conditions on 2D cell surface.

(A) Schematic illustration of hydrogel film coating on 2D cell surface. GC-T and HA-T hydrogel film were coated on 2D MIN6 β-cell. RITC was conjugated to GC-T and FA was used for HA-T. (B) Normalized fluorescence intensity of RITC and FA on cell surface measured by microplate reader. Coating conditions, which includes concentration of SA-Ty, SA-Ty reaction time, and concentration of polymers, were optimized to 0.05 U/ml SA-Ty, 10 min, 0.1% GC-T, and 0.1% HA-T.

set at 10 min, and the concentration of both polymers was 0.1%. The coating level increased with longer reaction time for coating of GC-T-RITC, where the concentration of SA-Ty was set at 0.05 U/ml and the concentration of both polymers was 0.1%. Finally, the RITC intensity sharply increased from 0.05% to 0.1%. However, the fluorescence intensity of FA showed insignificant change depending on coating conditions. To figure this out, the effect of SA-Ty reaction and electrostatic force on the hydrogel film coating was investigated (Fig. 2.9). The presence of SA-Ty increased the coating level of GC-T-RITC by 2.9 times, while the coating of HA-T-FA showed a nonsignificant increase (Fig 2.9.A). Next, the efficiency of HA-T coating was investigated by comparing the single HA-T film with the coating of HA-T film on GC-T film-coated cell (Fig. 2.9.B). The FA intensity showed 2.4 times higher when HA-T film was coated on GC-T film-coated cells. Additionally, GC-T film coated Jurkat cells formed much less clumps in the GC-T concentration of 0.1% because GC-T film on cell surface induced repulsion (Fig 2.10).

2.3.4 Identification of LbL hydrogel film by Quartz Crystal Microbalance

Based on the piezoelectric properties of the quartz crystal, the changes in oscillation frequency were measured in response to the deposition of hydrogel film on Cr/Au crystal (Fig. 2.11) [23, 24]. After inducing negative charge on Cr/Au crystal via O_2 plasma treatment, 0.1% GC-T solution and 0.1% HA-T solution in PBS were deposited on the crystal with or without SA-Ty. The accumulative mass can be calculated by following equation (Eqn. 1)

$$\Delta f = -C_f \cdot \Delta m \qquad \text{(Eqn. 1)}$$

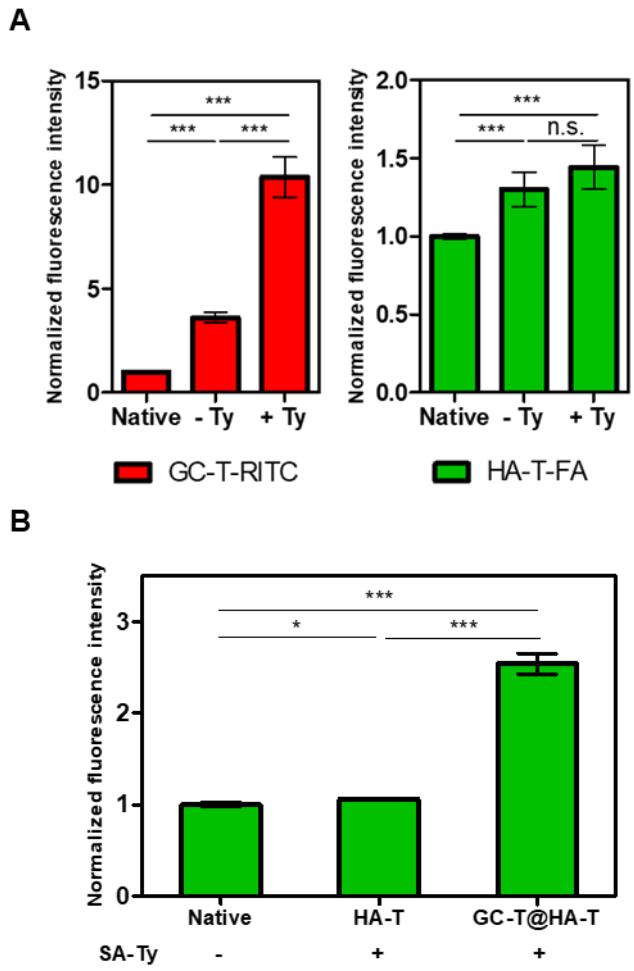

Figure 2.9 Comparison of the effect of SA-Ty and electrostatic force on hydrogel film coating.

Fold change of fluorescence intensity showed that (A) SA-Ty promoted the hydrogel film formation on the cell surface, more efficiently for GC-T than HA-T, and (B) HA-T film was formed more when GC-T film was precoated.

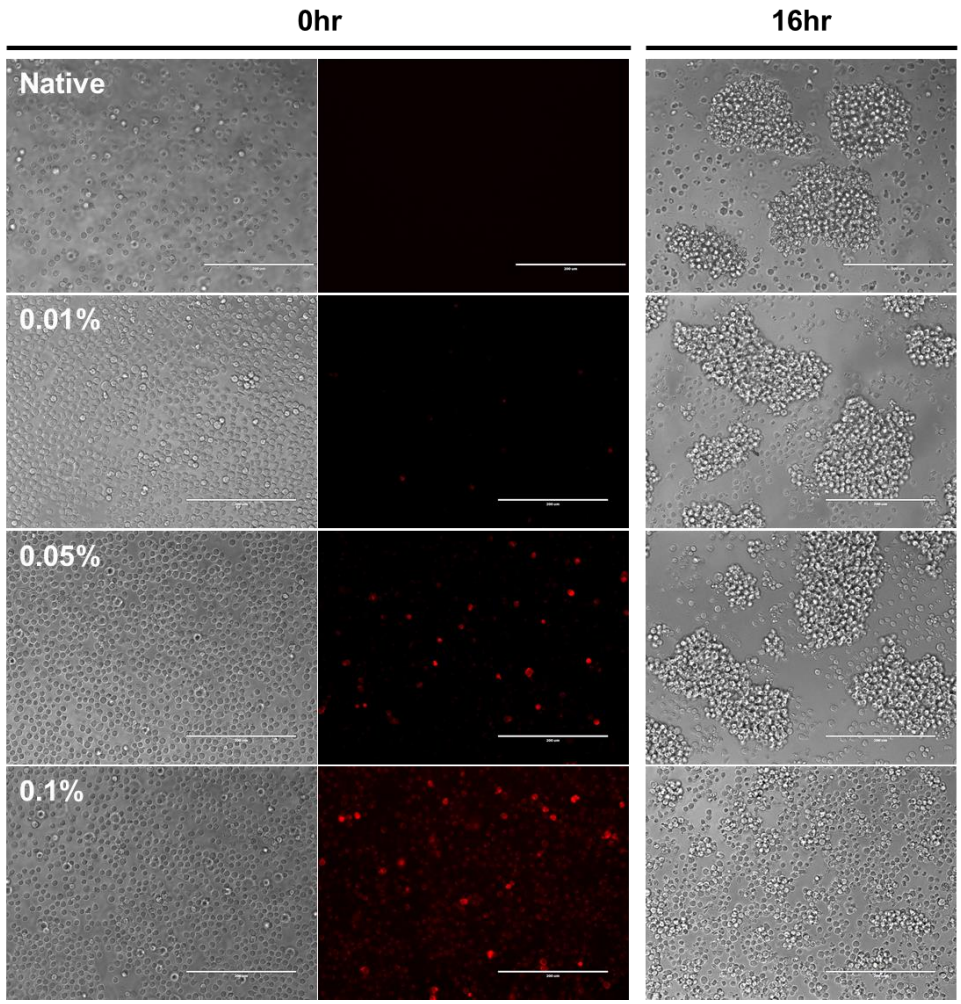

Figure 2.10 Cell clumping was inhibited by GC-T film coating at the concentration of 0.1%.

Jurkat cells, which form clumps, were coated with GC-T film and incubated for 16 h. 0.01%, 0.05%, and 0.1% indicate the concentration of GC-T solution used. 0.05 U/ml SA-Ty was reacted for 10 min in all groups. GC-T film coated Jurkat cells formed less clumps in 0.1% group while 0.01% and 0.05% groups showed large clumps.

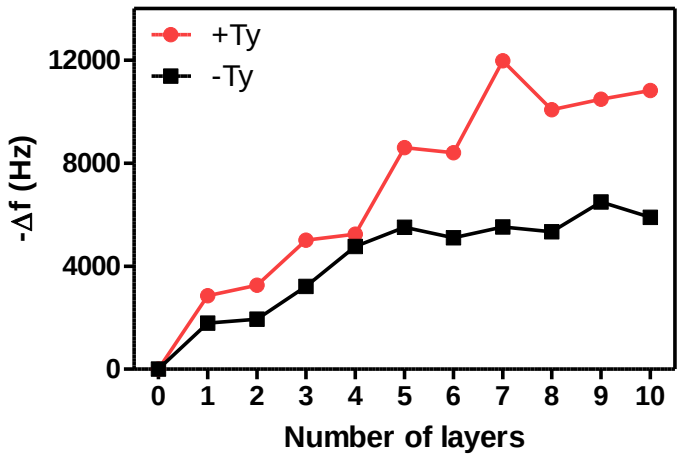

Figure 2.11 QCM analysis of layer-by-layer deposited hydrogel film.

where

Δf = the observed frequency change in Hz

Δm = the change in mass per unit area in g/cm2

C_f = the sensitivity factor for the crystal (56.6 Hz μg-1 cm2 for a 5 MHz AT-cut quartz crystal at RT)

At the layer of 6, the cumulative mass per area of hydrogel film was 90.16 and 148.50 μg/cm^2 for without and with SA-Ty, respectively, which shows 1.6 times heavier with SA-Ty. Furthermore, the mass per area of hydrogel film of 10 layers formed with SA-Ty was 191.27 μg/cm^2, which is 1.8 times higher than 104.24 μg/cm^2 of the 10-layer film formed without SA-Ty.

2.3.5 Identification of LbL hydrogel film-coated single cells

The coating platform was designed using a membrane with a pore smaller than the cell size to form a hydrogel film of multiple layers of the single cell surface (Fig. 2.12). The insert of Transwell® with 3.0 μm pore size was used to hold cells. Then, single cell coating was performed by dipping the cell-loaded insert into the coating solutions, medium, and PBS, sequentially. For the order of coating, positively charged polymer GC-T was applied first, and then HA-T and GC-T were coated alternately. The zeta potential of cells changed accordingly with the deposition of positively and negatively charged polymers (Fig. 2.13). The degree of coating was also evaluated by FACS analysis (Fig. 2.14). RITC of GC-T-RITC was detected in the channel of phycoerythrin (PE) and FA of HA-T-FA was detected in the channel Dotted box in (A) and (D) were magnified in (B) and (E), also (B) and (E) in (C) and (F). of fluorescein isothiocyanate

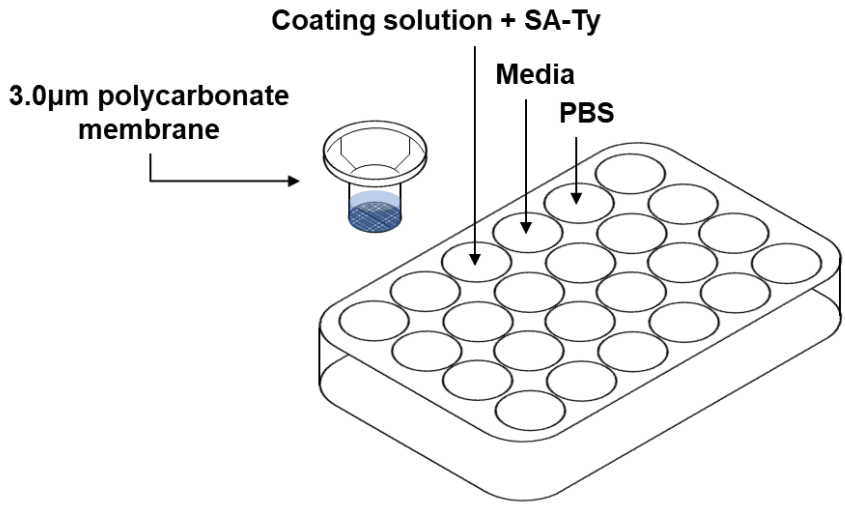

Figure 2.12 Schematic illustration of layer-by-layer cell coating with hydrogel film.

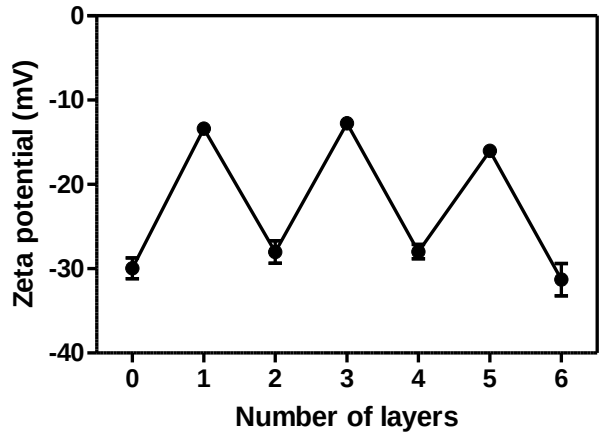

Figure 2.13 Zeta potential of layer-by-layer hydrogel film-coated single cells.

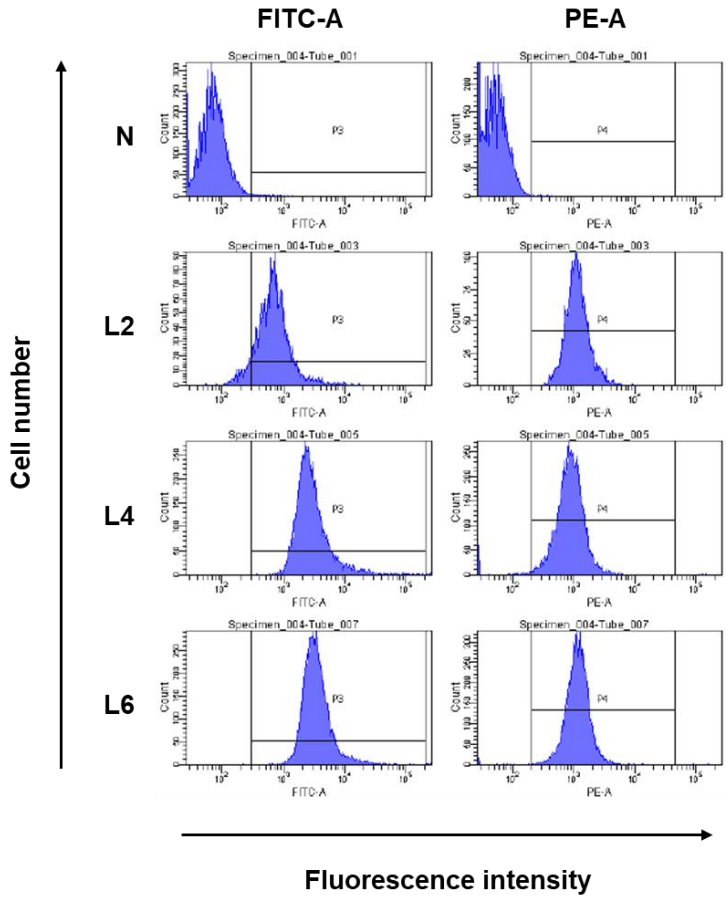

Figure 2.14 FACS analysis of layer-by-layer hydrogel film-coated single cells.

RITC of GC-T-RITC was detected in the channel of phycoerythrin (PE) and FA of HA-T-FA was detected in the channel of fluorescein isothiocyanate (FITC).

(FITC). The cell population was shifted to the region of stronger fluorescence intensity as layers were deposited. 6-layer coated Jurkat cells were imaged by CLSM (Fig. 2.15). Next, the GC-T/HA-T hydrogel film on the cell surface was observed directly using TEM (Fig. 2.16). The thickness of 6-layer hydrogel film was measured to be 139.40 ± 7.73 nm, which is considerably thicker than the previously reported LbL coating methods that depend only on the electrostatic force [13, 23, 24].

2.3.6 Cell viability and proliferation of hydrogel film-coated cells

Cell viability measured by staining cells with calcein-AM and ethidium homodimer-1 (EthD-1) (Fig. 2.17.A, B). The viability of hydrogel film-coated cells was over 99% on day 0 and 97% on day 1. Cell proliferation was investigated by measuring metabolic activity of cells using alamarBlue (Fig. 2.17.C). The total amount of metabolism steadily increased until day 4.

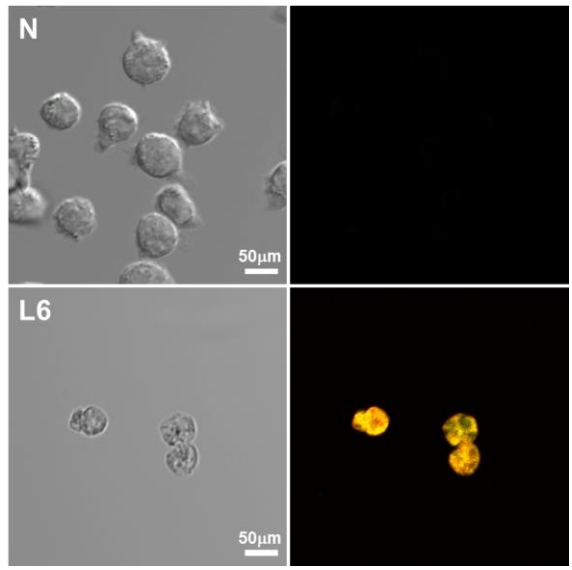

Figure 2.15 Confocal microscopic images of the hydrogel film-coated Jurkat cells.

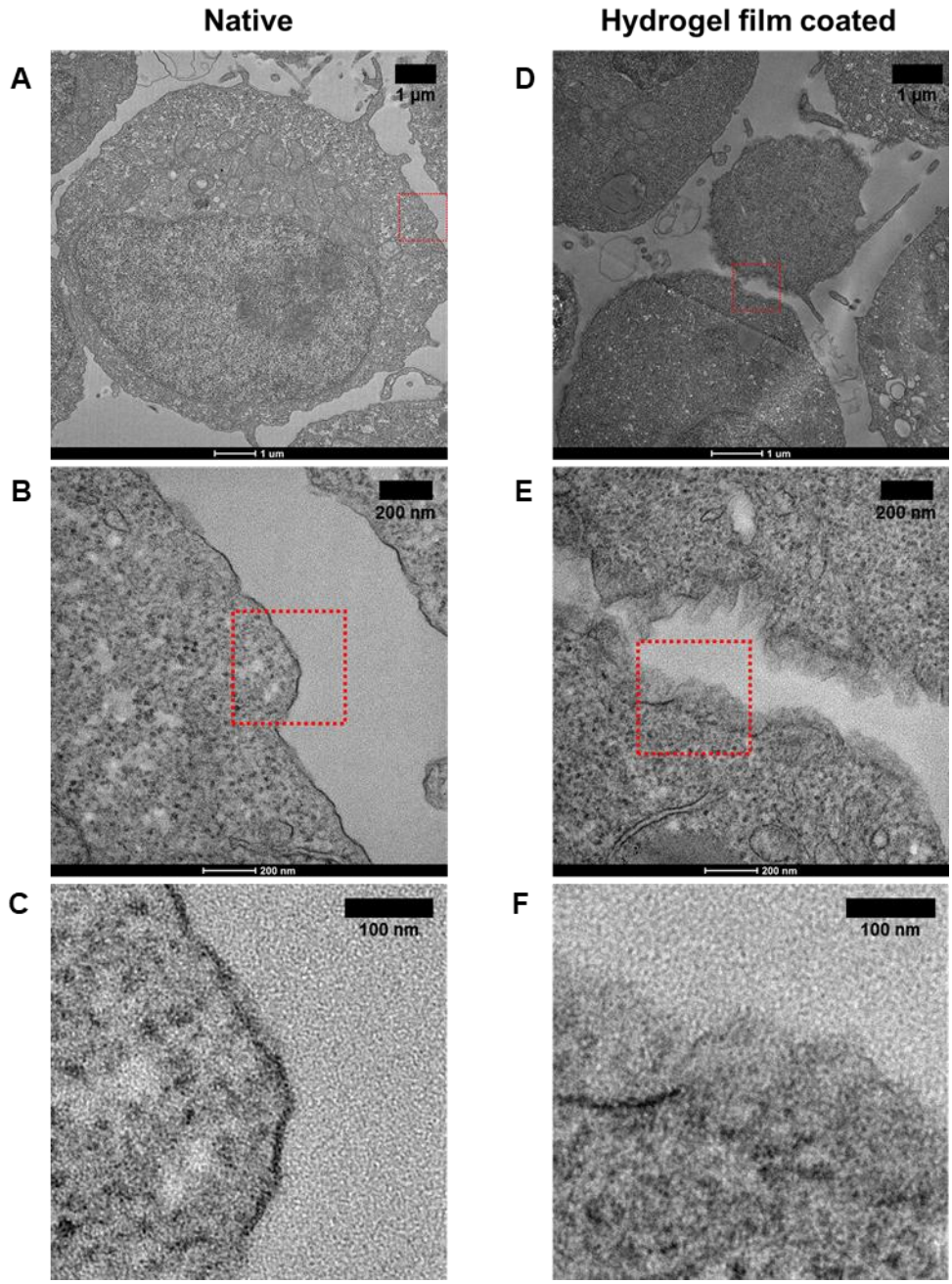

Figure 2.16 TEM images of the Jurkat cell membrane with and without hydrogel film.

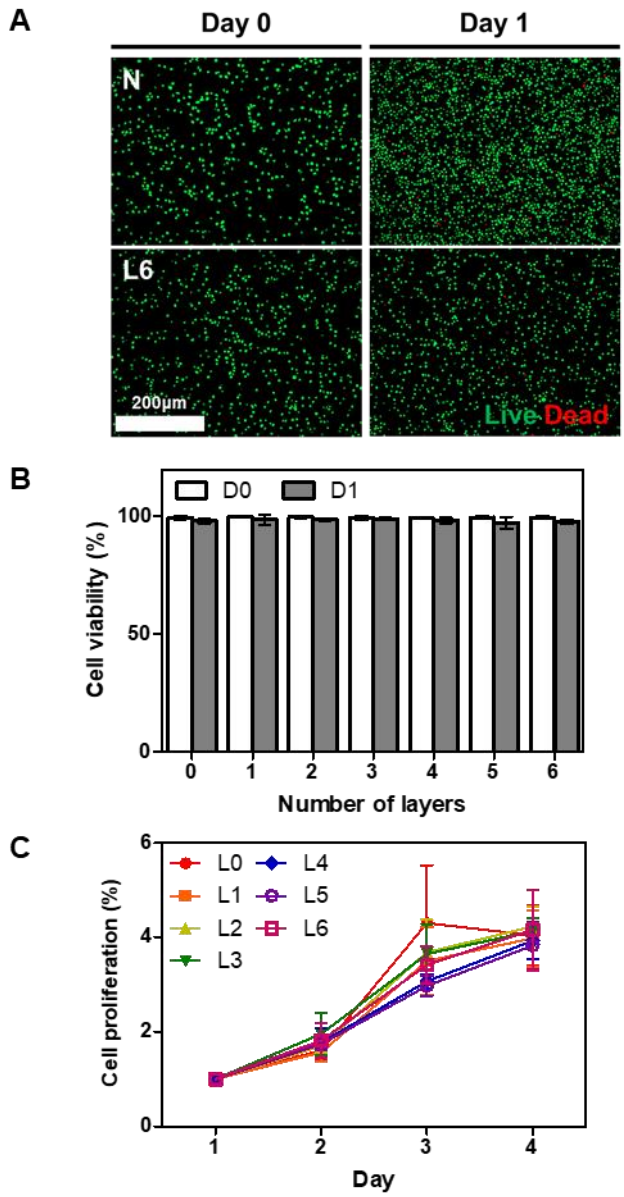

Figure 2.17 Cell viability and proliferation of hydrogel film-coated Jurkat cells.

(A) Calcein-AM was used to stain live cells, and dead cells were stained by ethidium homodimer-1 (EthD-1). (B) Cell viability was calculated by counting live cells in (A) (n=4). (C) Cell proliferation was measured by detecting cell metabolism at 24 h intervals using alamarBlue.

Chapter 3. Layer-by-layer (LbL) Coating of β-cell Spheroids for Islet Encapsulation

3.1 Introduction

Type 1 diabetes (T1D) is an autoimmune disease characterized by the destruction of β-cells by own immune cells, resulting in high blood glucose level due to the deficiency of insulin [25, 26, 27]. In the past, the treatment for T1D was implemented by daily injection of insulin. However, this method was invasive and inconvenient. The first pancreatic islet transplantation was attempted in 1893 [3]. After the establishment of Edmonton protocol, in which islet cells were isolated from brain-dead donors, in 2000, islet transplantation therapy has significantly improved. Nevertheless, 1) lack of cell source and supply of donated pancreas, 2) low cell survival due to the diffusion problem of oxygen and nutrients, 3) host immune rejection of the transplant and the harmful side effect from the administration of immunosuppressants are still major challenges of islet transplantation. Therefore, 1) development of β-cell like cells derived from stem cells, 2) downscaling the size of the capsule from macroscopic to micro- or nano-scopic encapsulation, 3) research for reducing immune rejection via developing less immunogenic biomaterials to inhibit the interaction between transplant β-cells and host immune cells or localized delivery of immunosuppressant to transplant site could be effective approach in the therapy for T1D [28-31].

3.2 Materials and methods

3.2.1 Fabrication of MIN6 β-cell spheroids and layer-by-layer hydrogel film coating

To fabricate β-cell spheroids, MIN6 pancreatic β-cells were detached from tissue culture plate with 0.25% trypsin-EDTA. Then, the cells were seeded into an ultra-low attachment 96-well plate (Corning, USA) at a density of 5×10^3 cells/well in 100 ul of culture medium and incubated in 5% CO2 at 37 °C for 3 days. The assembled spheroids were collected in 15 ml conical tubes and washed twice with PBS. 100 spheroids were placed on the 3.0 μm polycarbonate membrane and proceeded LbL encapsulation in the same manner as single cell encapsulation. After encapsulation, β-cell spheroids were transferred to a sterile 35 mm dish in culture medium.

3.2.3 Confocal laser scanning microscopy (CLSM)

After encapsulated with GC-T-RITC and HA-T-FA, β-cell spheroids were fixed with 4% PFA for 15 min at RT. The spheroids were placed on a 20 mm confocal dish. Imaging was performed via confocal microscope (LSM 780, Carl Zeiss, Germany)

3.2.4 Glucose-stimulated insulin secretion (GSIS) assay

Glucose-stimulated insulin secretion (GSIS) test was performed to evaluate the β-cell

functionality. β-cell spheroids were washed twice with D-PBS and incubated in 500ul of D-PBS for 1 h in 5% CO2 at 37 °C. After 1 h, low-glucose solution (3.3 mM glucose in D-PBS) and high-glucose solution (20 mM glucose in D-PBS) was treated to different groups and incubated for 2 h in a 37 °C incubator. The supernatants of glucose solution, which contain secreted protein of insulin, were collected from each well. The amount of insulin was measured via mouse insulin enzyme-linked immunosorbent assay (Mouse Insulin ELISA, ALPCO, NH, USA) according to the manufacturer's instructions. β-cell spheroids were lysed with 0.2% triton X-100 in TE buffer for 30 min with voltexing every 5 min. PicoGreen® assay was performed to quantitate dsDNA of the cells in whole spheroids to standardize the secreted insulin level. The stimulation index (SI) was calculated as the amount of the insulin level at high-glucose condition divided by the insulin level at low-glucose condition.

3.2.5 Physical stress test

For physical stress test, β-cell spheroids were dispersed in 500 ul of PBS in 1.7 ml Eppendorf tube after washing twice in PBS. Tabletop centrifuge (MiniSpin Plus, Eppendorf, Germany) was used to centrifuge spheroids at 1,100 and 4,000 rpm for 5 min. Between each step of centrifugation, clustered spheroids were resuspended without changes in PBS. After 3 times, residual cell traces are stained with calcein-AM and EthD-1 and imaged with fluorescence microscope.

3.2.6 Oxidative stress test

Three β-cell spheroids were placed on each 96-well black plate well in 50 ul of media. Then, 50 ul of 4, 2, 1, 0 mM H_2O_2 solution were spread to make final concentration of 2, 1, 0.5, 0 mM H_2O_2 in media. β-cell spheroids were incubated for 30 min at RT. After 30 min, 100 ul of CellTiter Glo® was added to each well. The plate was shaken on the orbital shaker for 2 min and incubated at RT in order to stabilize the luminescent molecules. The intensity of luminescence was measured by microplate reader for 1000 ms.

3.2.7 Statistical analysis

All data are expressed as mean ± standard deviation (SD). Statistical significance was determined by Student's t-test with * $p < 0.05$, ** $p < 0.01$, *** $p < 0.005$.

3.3 Results & Discussion

3.3.1 Layer-by-layer hydrogel film coating of β-cell spheroids

MIN6, a mouse pancreatic insulinoma cell line, β-cell spheroids were spontaneously assembled by culturing cells on ultra-low attachment plates (Fig. 3.1). A β-cell spheroid was found to average 350.0 ± 24.5 μm in diameter, as measured for 20 spheroids at 4 locations each (Fig. 3.2). β-cell spheroids were coated with hydrogel film via the coating platform designed in Chapter 2. The hydrogel film on the spheroids was visualized by labeling coating polymers with fluorescent dyes. According to the fluorescent images and intensity measurements, the hydrogel film layer was further coated with layer deposition (Fig 3.3). CLSM images showed thin, uniform, and compact film layers on β-cell surface (Fig 3.4).

3.3.2 Cell viability of hydrogel film-coated β-cell spheroids

Cell viability was evaluated by staining β-cell spheroids with calcein-AM and EthD-1 (Fig. 3.5.A). Most of the cells were alive for 7 days, both N and L6, and only a few dead cells were observed in the center of the spheroids. The size and density of β-cell spheroids increased with time. Additionally, cell proliferation was maintained, as examined by alamarBlue assay (Fig. 3.5.B).

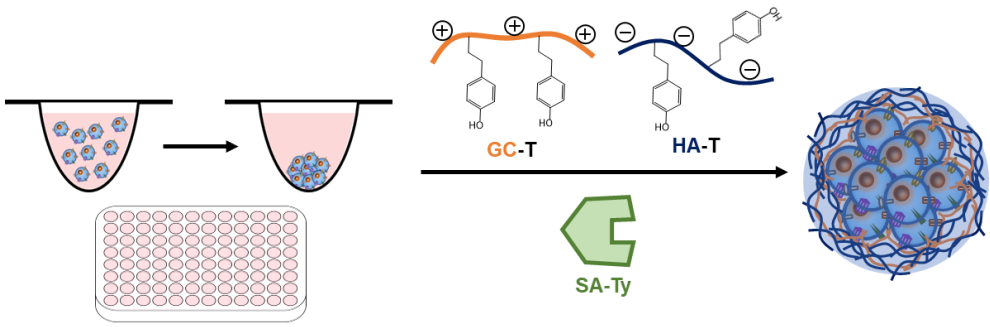

Figure 3.1 Schematic illustration of layer-by-layer hydrogel film coating of β-cell spheroids.

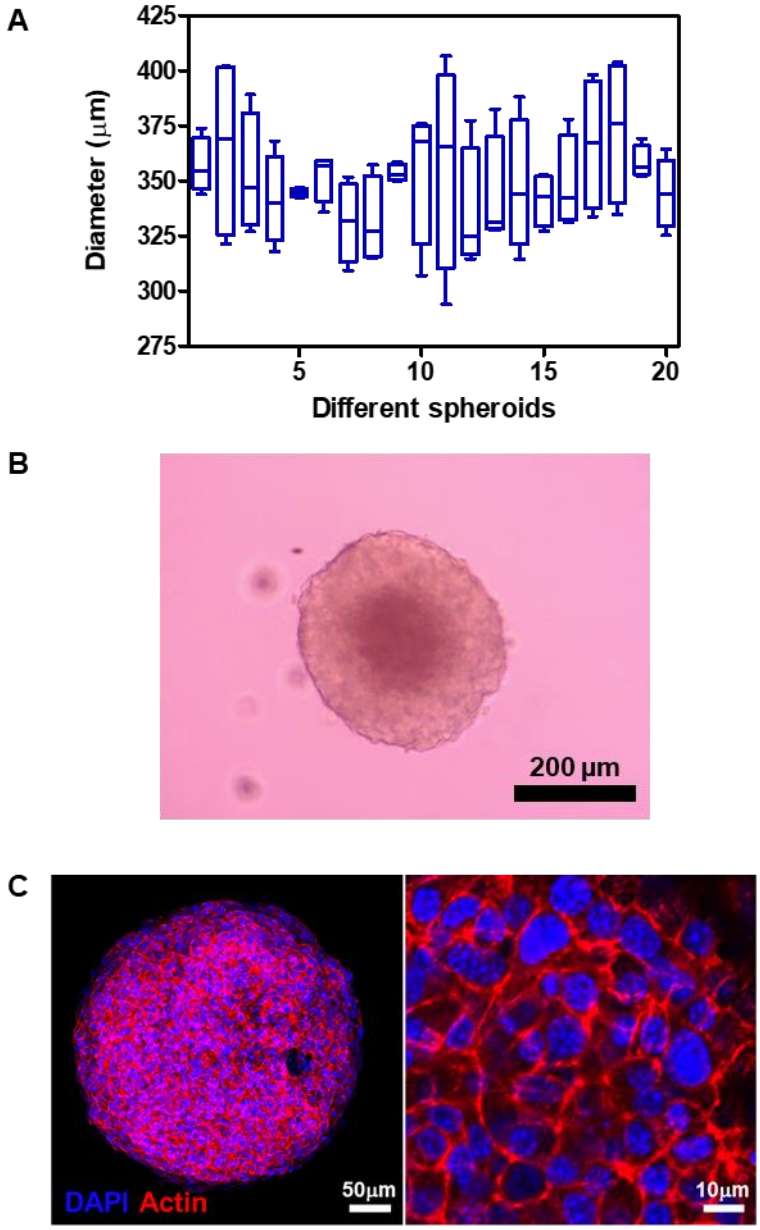

Figure 3.2 Size of β-cell spheroids, measured at multiple locations across spheroids, for 20 spheroids.

(A) The box and whisker plot was assessed by Tukey's method. (B) Optical microscopic image of a β-cell spheroid.

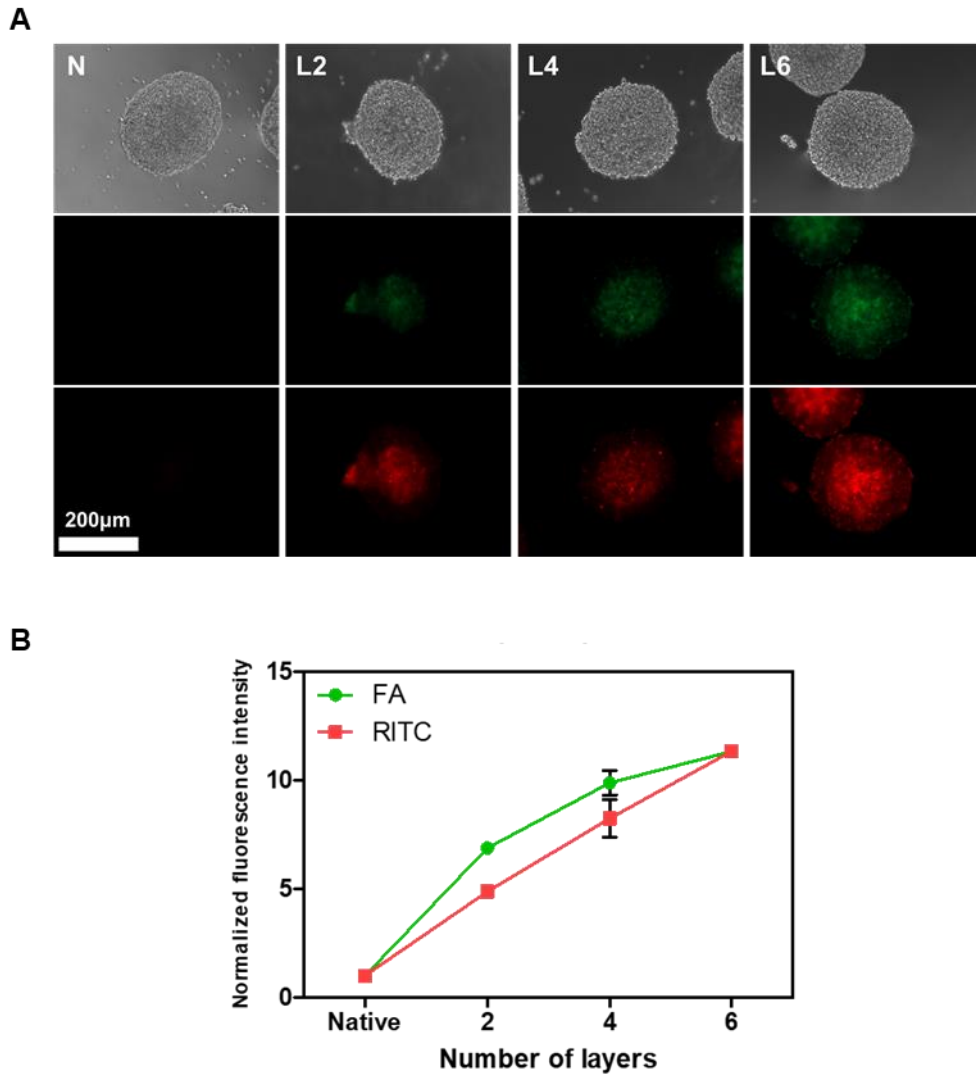

Figure 3.3 Layer-by-layer hydrogel film coating of β-cell spheroids.

(A) Fluorescence microscopic images of β-cell spheroids coated with hydrogel film in different number of layers. (B) The intensity of fluorescence of hydrogel film-coated β-cell spheroids.

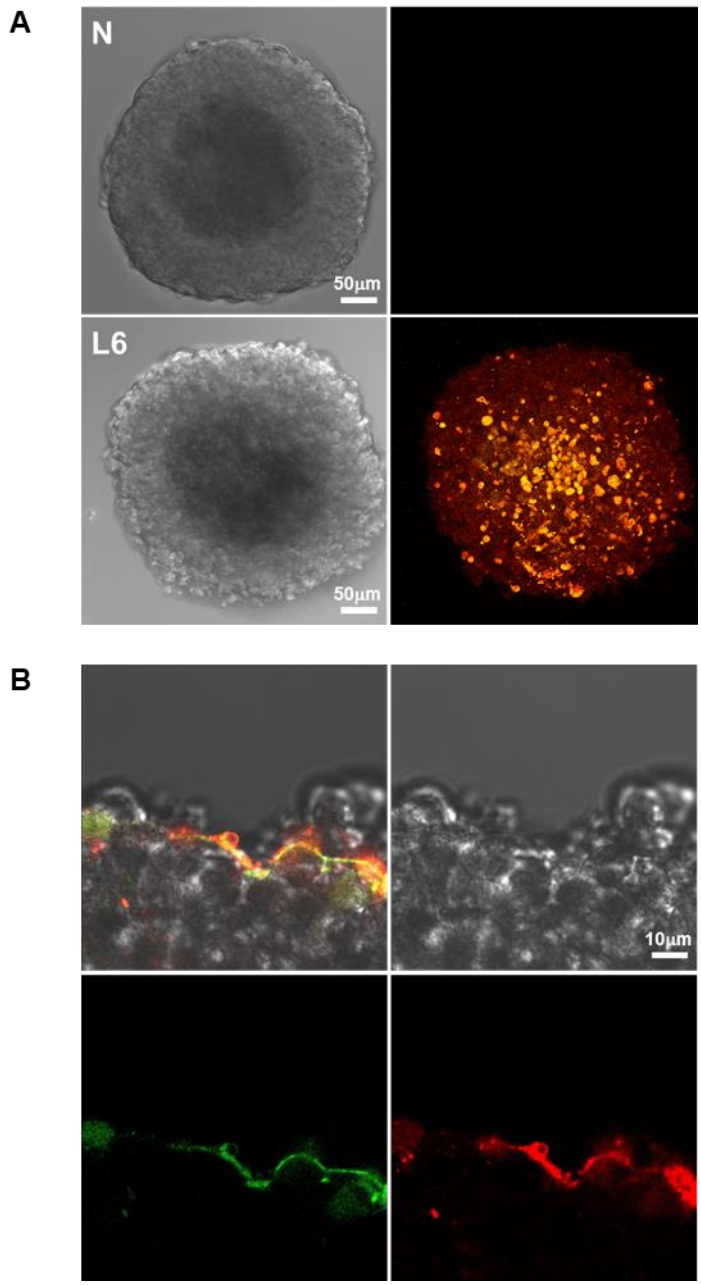

Figure 3.4 Confocal microscopic images of the hydrogel film-coated β-cell spheroids.

(A) Comparison of native and 6-layer coated spheroids. (B) Magnified images of 6-layer coated spheroids.

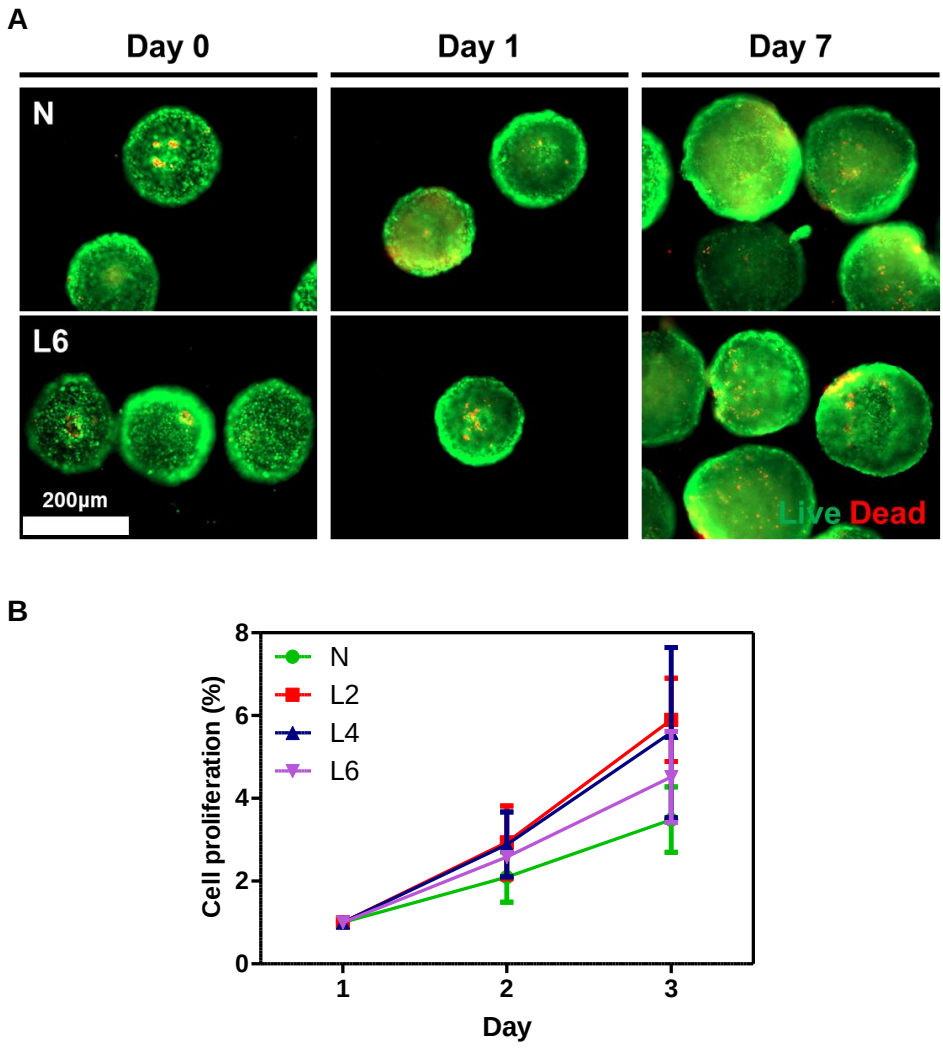

Figure 3.5 Cell viability and proliferation of hydrogel film-coated β-cell spheroids.

(A) Live/Dead staining images for 7 days. (B) Cell proliferation measured by alamarBlue assay for 3 days.

3.3.3 Evaluation of the functionality of hydrogel film-coated β-cell spheroids

To evaluate the cellular functionality after coating with hydrogel film, glucose-stimulated insulin secretion (GSIS) assay was performed for native (N) and 6-layer coated (L6) β-cell spheroids (Fig. 3.6). The β-cell spheroids were induced to secrete insulin in response to the different concentrations of glucose in D-PBS. Insulin level was obtained by dividing the total amount of secreted insulin by the amount of DNA. Stimulation index (SI) was calculated by dividing the insulin level at high-glucose solution by the insulin level at low-glucose solution. Insulin levels at low-glucose solution of N and L6 were similar, while the level of L6 was significantly higher than N at high-glucose solution. Accordingly, the SI of L6 was 4.1 times higher than that of N.

3.3.4 Cytoprotection effect against physical stress

Morphology of β-cell spheroids was evaluated by brightfield microscopy (Fig. 3.7). Native and 6-layer coated β-cell spheroids were centrifugated at 1,100 and 4,000 rpm (81 x g and 1,073 x g, respectively) In 1,100 rpm, β-cell spheroids in both groups maintained the spherical shape. However, in 4,000 rpm, 6-layer coated β-cell spheroids were protected, while native spheroids were almost smashed.

3.3.5 Cytoprotection effect against oxidative stress

Cell viability of β-cell spheroids were assessed by CellTiter Glo® ATP-measuring luminescent reagent (Fig. 3.8). Native and 6-layer coated β-cell spheroids were picked by careful suction using a micropipette. β-cell spheroids were incubated in H_2O_2 solution for 30 min and the level of ATP was obtained. In 0.5 and 1 mM of H_2O_2 solution, the hydrogel film-coated group showed higher viability than the native significantly. However, in 2 mM of H_2O_2, both groups showed viability of less than 10%, which were non-significantly different.

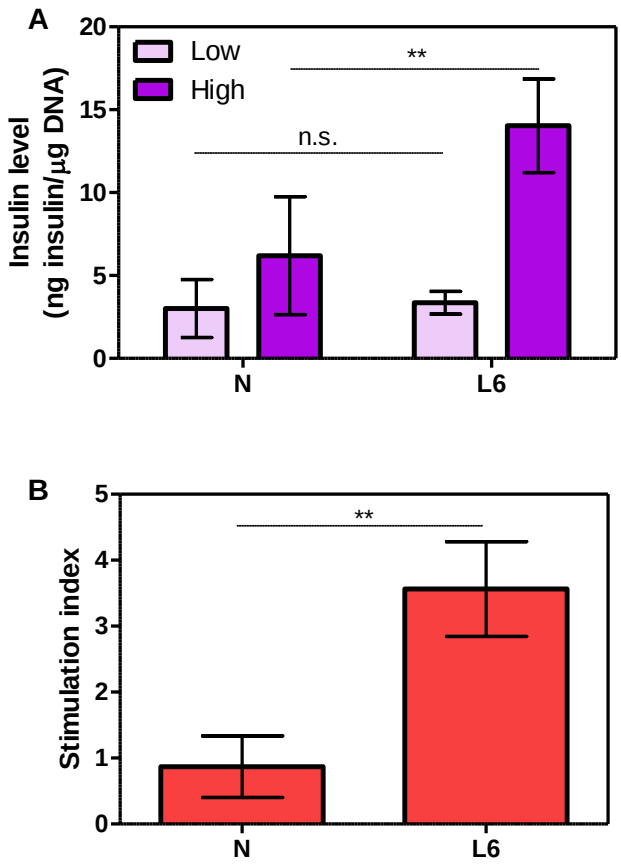

Figure 3.6 Functionality of hydrogel film-coated β-cell spheroids.

(A) Glucose-stimulated insulin secretion (GSIS) assay of β-cell spheroids at low (3.3 mM; light purple bar) and high (20 mM; deep purple bar) concentrations of glucose (n=3). (B) Stimulation index (SI) of GSIS test for native and 6-layer coated β-cell spheroids (n=3).

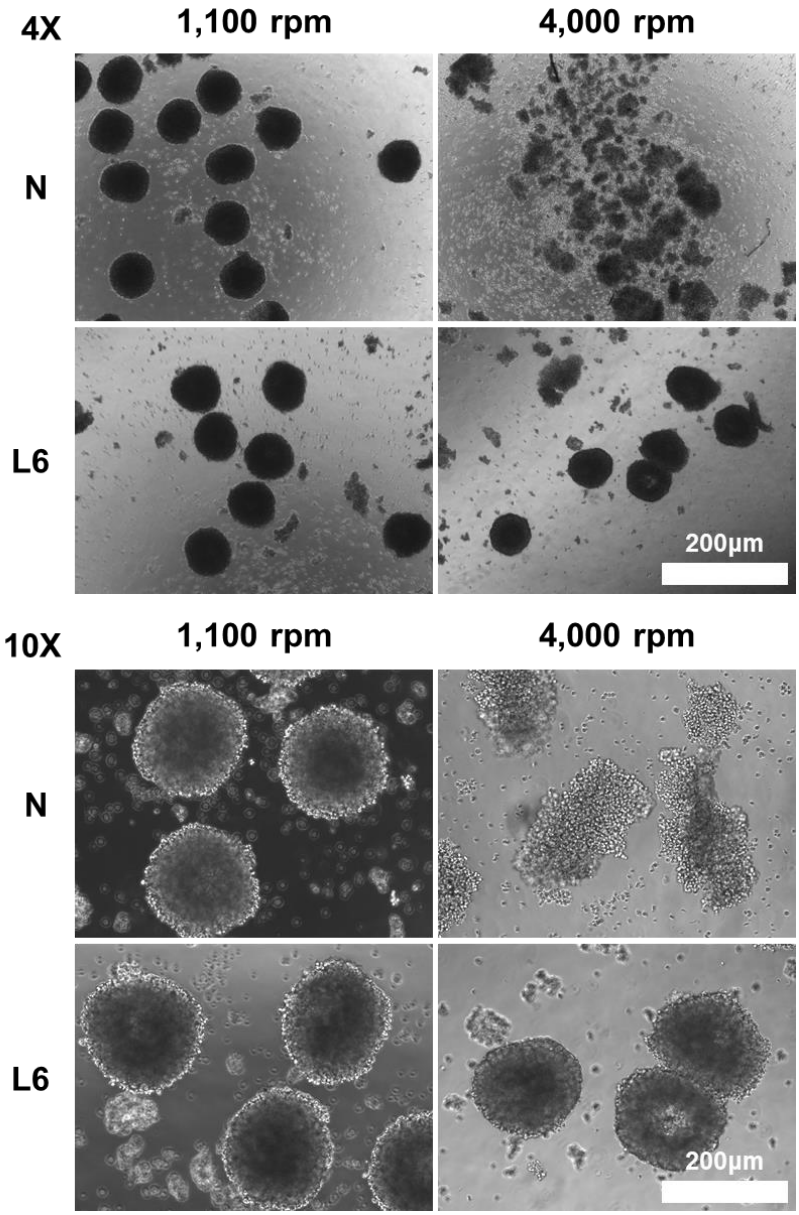

Figure 3.7 Cytoprotection effect against physical stress.

Native or 6-layer coated β-cell spheroids were stained with Live/Dead reagents after centrifugation at 1,100 rpm and 4,000 rpm.

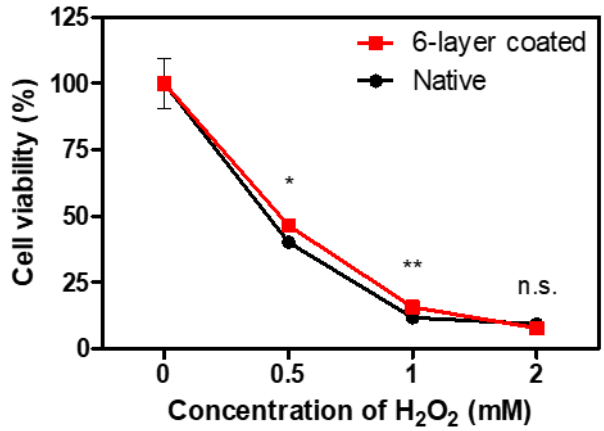

Figure 3.8 Cytoprotection effect against oxidative stress.

Chapter 4. Conclusions

We have constructed a layer-by-layer cell coating platform using mono-phenolic group-conjugated glycol chitosan and hyaluronic acid via tyrosinase mediated oxidative coupling reactions. The polymers and recombinant tyrosinase protein were synthesized, characterized. The hydrogel film on cell surface was fabricated by immersing the cell-mounted membrane in and out of the coating solution. The 6-layer stacked hydrogel film was as thick as 139.40 nm which is remarkable figure compared to previous layer-by-layer cell coating studies. Furthermore, β-cell spheroids were coated with the hydrogel film as well. Cell viability was not deteriorated by cell coating process. Meanwhile, glucose sensitivity of the β-cell spheroids was enhanced by hydrogel film coating. External stress, including physical and oxidative stress, was caused to hydrogel film-coated β-cell spheroids to test the resistance to harsh environments that exist when delivering therapeutic cells *in vivo*. Altogether, our results describe a novel cell encapsulation technique which have a potential as a general platform to be applied in various types of cell therapy.

References

[1] Mitrousis, N., et al. (2018). "Biomaterials for cell transplantation." Nature Reviews Materials **3**(11): 441-456.

[2] Abbina, S., et al. (2017). "Surface Engineering for Cell-Based Therapies: Techniques for Manipulating Mammalian Cell Surfaces." ACS Biomaterials Science & Engineering **4**(11): 3658-3677.

[3] Farina, M., et al. (2018). "Cell encapsulation: Overcoming barriers in cell transplantation in diabetes and beyond." Adv Drug Deliv Rev.

[4] Tang, J., et al. (2017). "Heart Repair Using Nanogel-Encapsulated Human Cardiac Stem Cells in Mice and Pigs with Myocardial Infarction." ACS Nano **11**(10): 9738-9749.

[5] Hasturk, O. and D. L. Kaplan (2018). "Cell armor for protection against environmental stress: Advances, challenges and applications in micro- and nanoencapsulation of mammalian cells." Acta Biomater.

[6] Fang, R. H., et al. (2018). "Cell Membrane Coating Nanotechnology." Adv Mater **30**(23): e1706759.

[7] Pham-Hua, D., et al. (2017). "Islet encapsulation with polyphenol coatings

decreases pro-inflammatory chemokine synthesis and T cell trafficking." Biomaterials **128**: 19-32.

[8] Kozlovskaya, V., et al. (2012). "Ultrathin polymeric coatings based on hydrogen-bonded polyphenol for protection of pancreatic islet cells." Adv Funct Mater **22**(16): 3389-3398.

[9] Zhu, W., et al. (2019). "SupraCells: Living Mammalian Cells Protected within Functional Modular Nanoparticle-Based Exoskeletons." Adv Mater: e1900545.

[10] Pham, T. T., et al. (2018). "Tissue adhesive FK506-loaded polymeric nanoparticles for multi-layered nano-shielding of pancreatic islets to enhance xenograft survival in a diabetic mouse model." Biomaterials **154**: 182-196.

[11] Mao, A. S., et al. (2017). "Deterministic encapsulation of single cells in thin tunable microgels for niche modelling and therapeutic delivery." Nat Mater **16**(2): 236-243.

[12] Park, J., et al. (2018). "Engineering the Surface of Therapeutic "Living" Cells." Chem Rev **118**(4): 1664-1690.

[13] Yang, J., et al. (2019). "Encapsulation of individual living cells with enzyme responsive polymer nanoshell." Biomaterials **197**: 317-326.

[14] Wilson, J. T., et al. (2011). "Cell surface engineering with polyelectrolyte

multilayer thin films." J Am Chem Soc **133**(18): 7054-7064.

[15] Kim, H., et al. (2018). "General and Facile Coating of Single Cells via Mild Reduction." J Am Chem Soc **140**(4): 1199-1202.

[16] Rogozhnikov, D., et al. (2016). "Scaffold Free Bio-orthogonal Assembly of 3-Dimensional Cardiac Tissue via Cell Surface Engineering." Sci Rep **6**: 39806.

[17] Youn, W., et al. (2017). "Cytoprotective Encapsulation of Individual Jurkat T Cells within Durable TiO2 Shells for T-Cell Therapy." Angew Chem Int Ed Engl **56**(36): 10702-10706.

[18] Niu, J., et al. (2017). "Engineering live cell surfaces with functional polymers via cytocompatible controlled radical polymerization." Nat Chem **9**(6): 537-545.

[19] P. de Vos, et al. (2014). "Polymers in cell encapsulation from enveloped cell perspective." Adv Drug Deliv Rev **67-68**: 15-34.

[20] Lee, S. H., et al. (2016). "Using tyrosinase as a monophenol monooxygenase: A combined strategy for effective inhibition of melanin formation." Biotechnol Bioeng **113**(4): 735-743.

[21] Kim, S. H., et al. (2018). "Enzyme-mediated tissue adhesive hydrogels for meniscus repair." Int J Biol Macromol **110**: 479-487.

[22] Kim, S. H., et al. (2018). "Tissue adhesive, rapid forming, and sprayable ECM hydrogel via recombinant tyrosinase crosslinking." Biomaterials **178**: 401-412.

[23] Choi, D., et al. (2017). "Multifunctional Collagen and Hyaluronic Acid Multilayer Films on Live Mesenchymal Stem Cells." ACS Appl Mater Interfaces **9**(14): 12264-12271.

[24] Choi, D., et al. (2017). "Cytoprotective Self-assembled RGD Peptide Nanofilms for Surface Modification of Viable Mesenchymal Stem Cells." Chemistry of Materials **29**(5): 2055-2065.

[25] Zhou, Q. and D. A. Melton (2018). "Pancreas regeneration." Nature **557**(7705): 351-358.

[26] Vegas, A. J., et al. (2016). "Long-term glycemic control using polymer-encapsulated human stem cell-derived beta cells in immune-competent mice." Nat Med **22**(3): 306-311.

[27] Bochenek, M. A., et al. (2018). "Alginate encapsulation as long-term immune protection of allogeneic pancreatic islet cells transplanted into the omental bursa of macaques." Nat Biomed Eng **2**(11): 810-821.

[28] Fukuda, Y., et al. (2018). "Layer-by-layer cell coating technique using extracellular matrix facilitates rapid fabrication and function of pancreatic beta-cell spheroids." Biomaterials **160**: 82-91.

[29] Wilson, J. T., et al. (2008). "Layer-by-layer assembly of a conformal nanothin PEG coating for intraportal islet transplantation." Nano Lett **8**(7): 1940-1948.

[30] Kizilel, S., et al. (2010). "Encapsulation of pancreatic islets within nano-thin functional polyethylene glycol coatings for enhanced insulin secretion." Tissue Eng Part A **16**(7): 2217-2228.

[31] Llacua, L. A., et al. (2018). "Extracellular matrix molecules and their potential contribution to the function of transplanted pancreatic islets." Diabetologia **61**(6): 1261-1272.

국문초록

세포치료제를 위한 적층식 하이드로겔 필름 세포 코팅

세포치료제는 중증 질환에 대한 치료법으로 주목을 받고 있다. 하지만, 세포치료제의 효능은 주사 시 또는 투여 후 외부 스트레스로 인해 그 생존율이 낮다는 한계점이 있다. 본 연구에서는 생체 적합 및 세포 보호 하이드로겔 필름을 사용하여 적층식 세포 코팅 플랫폼을 구축하였다. 하이드로겔 막 형성을 촉진하기 위하여, 반대 전하를 띄며 Streptomyces avermitilis 유래 타이로시네이즈 매개 산화 커플링 반응을 통해 세로 표면의 작용기와 공유결합을 형성하거나 교차결합하는 히알루론산 및 글라이콜 키토산에 단일페놀 그룹을 도입하였다. 하이드로겔 필름이 코팅된 세포는 제타 전위, 형광 세기를 측정하고 TEM 이미지를 측정하여 확인되었다. 6개 층이 쌓인 하이드로겔 필름은 139.40 nm였다. 코팅 과정 후 세포의 생존율은 나빠지지 않았다. 더 나아가, 췌도 이식에의 활용을 위하여 베타 세포 스페로이드의 표면에 하이드로겔 필름을 형성하였다. 컨포칼 이미지에서 얇고, 균일하고, 압축되어 있는 필름 층을 관찰할 수 있었다. 더욱이, 하이드로겔 필름이 코팅된 베타 세포 스페로이드는 일반 세포보다 더 높은 인슐린 분비 능력을 보였다. 마지막으로, 하이드로겔 필름의 물리적, 산화 스트레스에 대한 세포 보호 효과가 확인되었다. 따라서, 우리가 개발한 빠르고, 편리하고, 단단하고, 층 수 제어가 가능한 세포 코팅 기술이 세포치료제의 임상 활용에 있어 큰 잠재력을 부여할

것으로 기대한다.

주요어: 세포치료제, 세포 표면 공학, 췌도 이식, 세포 보호

학번: 2017-22285